

# Numerical Simulation of Decarburization Reaction with Oxygen Blowing During RH Refining Process



KAIYU PENG, CHANG LIU, LIFENG ZHANG, and YU SUN

A mathematical model for the decarburization coupling with the fluid flow in the RH refining process was established. The decarburization reaction at three sites was considered, including the surface of injection lifting gas bubbles, the gas–liquid interface in the vacuum chamber and the interior of the molten steel bath. The effect of the flow pattern on the transfer of carbon and oxygen in the molten steel was obtained. The decarburization inside the molten steel bath in the vacuum chamber contributed the most, accounting for 55.9 pct of the total decarburization. The gas–liquid interface in the vacuum chamber and the surface of bubbles injected from the up-leg snorkel contributed approximately 32.5 and 11.6 pct, respectively. The oxygen blowing through the top of the vacuum chamber promoted the decarburization of RH refining whenever the oxygen was injected. When the oxygen was injected at the beginning of the decarburization process, the contribution of the decarburization at the top surface of the molten steel in the vacuum chamber to the total decarburization increased from 11.6 to 28.3 pct.

<https://doi.org/10.1007/s11663-022-02519-0>

© The Minerals, Metals & Materials Society and ASM International 2022

## I. INTRODUCTION

THE RH (Ruhrstahl–Hereaus) refining process is usually used in the production of ultra-low carbon aluminum killed steel, supplemented by oxygen blowing operations, to achieve the purpose of deep decarburization and reduce the carbon content in molten steel to less than 20 ppm. The improvement of decarburization efficiency in the RH refining process is of great significance to the production of ultra-low carbon steel.

Based on the basic theory of metallurgical physical chemistry, through the combination with computer technology, there have been many reports on the coupling phenomenon of fluid flow and physicochemical reaction in the metallurgical process.<sup>[1,2]</sup> In the actual production process, thermodynamics can give whether the decarburization reaction can occur or not, while the reaction rate of the decarburization reaction is affected by kinetic factors, involving the mass transfer of carbon and oxygen in molten steel. As an important step in the production of ultra-low carbon steel, the mechanism and simulation of the decarburization process of RH have been concerned<sup>[3–5]</sup> and a large number of reports have been made on the decarburization reaction in various stages of the steelmaking process.<sup>[6–12]</sup>

In recent decades, there are researches on the flow and mixing phenomenon in the RH refining process, which includes both numerical modeling and experimental works. However, the numerical simulation application on the chemical reactions is relatively rare. In the study of decarburization reaction in the RH refining process, the existing models mainly discuss the thermodynamic and kinetic mechanism of decarburization.<sup>[13–17]</sup> Only few of them involve the coupling calculation of three-dimensional molten steel flow and carbon-oxygen mass transfer process.<sup>[5,18,19]</sup>

In the current work, based on the steady flow field of the RH refining process obtained from the previous numerical simulation, the decarburization reaction of the RH refining process is simulated by user-defined scalar (UDS) equation. The variation of carbon and

KAIYU PENG is with the School of Metallurgical and Ecological Engineering, University of Science and Technology Beijing (USTB), Beijing 100083, P.R. China and also with the Beijing Shougang Co., Ltd., Qian'an 064404, Hebei, P.R. China. CHANG LIU is with the State Key Laboratory of Refractories and Metallurgy, Wuhan University of Science and Technology, Wuhan, 430081 Hubei, P.R. China and also with the Key Laboratory for Ferrous Metallurgy and Resources Utilization of Ministry of Education, Wuhan University of Science and Technology, Wuhan, Hubei 430081, P.R. China. Contact e-mail: liuchang\_san@outlook.com LIFENG ZHANG is with the School of Mechanical and Materials Engineering, North China University of Technology, Beijing 100144, P.R. China. Contact e-mail: zhanglifeng@ncut.edu.cn YU SUN is with the School of Metallurgical and Ecological Engineering, University of Science and Technology Beijing (USTB).

Manuscript submitted September 14, 2021; accepted March 26, 2022.

Article published online April 16, 2022.

oxygen content in the molten steel was calculated, and the contribution of three reaction regions to decarburization reaction is analyzed.

## II. MULTIPHASE FLUID FLOW DURING RH REFINING PROCESS

### A. Modeling Descriptions

Firstly, the fluid flow during the RH refining process was calculated using the  $k-\varepsilon$  model. Based on the steady-state fluid flow, the decarburization reaction model considering three sites, bubbles surface, interior and the surface of the molten steel in the vacuum chamber was established.

The volume of fraction (VOF) model is adopted to simulate the multiphase flow, which is used to calculate the phase interface between molten steel and argon gas. The discrete phase model (DPM) is used to calculate the trajectory of argon bubbles and the interaction between argon bubbles and molten steel. The turbulent model is the  $k-\varepsilon$  model. The mesh and boundary conditions are shown in Figure 1. The total number of cells used in the calculation is about 480,000. The material properties and the dimensions of RH treatment used in the calculation are listed in Tables I and II. The detailed model parameters could be found in the authors' previous study.<sup>[20–23]</sup>

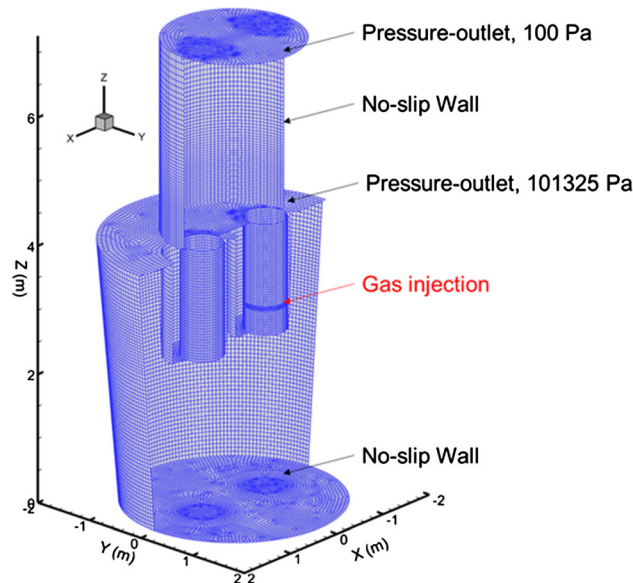


Fig. 1—Mesh and boundary conditions for simulation on steel-argon system of RH.

Table I. Material Properties for Calculation

Variable	Unit	Molten Steel	Argon Gas
Density	kg/m <sup>3</sup>	7020	0.34
Viscosity	kg/(m s)	$6.7 \times 10^{-3}$	$8.9 \times 10^{-5}$
Temperature	K	1873	
Interaction Force	N/m	1.84	

The assumptions concerned in the current calculation are as follows,

- The fluids, molten steel, and gas, are Newtonian, viscous, and incompressible.
- To simplify the model, the slag is neglected, considering there is almost no slag in the vacuum chamber.
- Bubbles are assumed to be spherical and their deformation, coalescence, and breakup are neglected.
- The fluid flow in the RH reactor is assumed to be an isothermal process. The temperature variation and its effect on the fluid flow are neglected.
- The decarburization process calculation is based on a steady-state flow field.

### B. Numerical Simulation Procedures

The simulation processing was performed using the ANSYS Fluent 17.0 commercial software, based on the finite volume method. The PISO algorithm was carried out for the pressure-velocity coupling. The spatial discretization for momentum used the second-order upwind method, and the transient formulation was second-order implicit. The convergence criterion for the continuity of momentum was  $10^{-5}$ . The calculation time step was 0.001 seconds.

### C. Fluid Flow and Bubbles Distribution

Figure 2 shows the distribution of three-dimensional velocity streamlines and turbulent kinetic dissipation rate of RH ladle and vacuum chamber. The steel level in the vacuum chamber is the iso-surface with a 0.7 volume fraction of molten steel. It can be seen that the velocity of molten steel in the snorkels is fast, and the fluid forms eddy in the ladle and vacuum chamber. When the argon gas is blown into the vacuum chamber, the free surface of the molten steel in the vacuum chamber is blown up to a certain height.

The bubble surface is another vital site for decarburization reaction during the RH refining process. Figure 3 shows the spatial distribution of movement velocity and residence time of argon bubbles during the argon

Table II. Dimensions of RH Reactor

Item	Dimensions
Diameter of Ladle Top (mm)	3959
Diameter of Ladle Bottom (mm)	3324
Height of Ladle (mm)	4060
Inner Diameter of Vacuum Chamber (mm)	2144
Height of Vacuum Chamber (mm)	8225
Length of Snorkels (mm)	1075
Inner Diameter of Gas Injection Nozzles (mm)	6
Diameter of Snorkels (mm)	650
Injection Gas Flow Rate (NL/min)	3000
Number of Gas Injection Nozzles	12
Pressure of Vacuum Chamber (Pa)	100
Immersion Depth (mm)	500

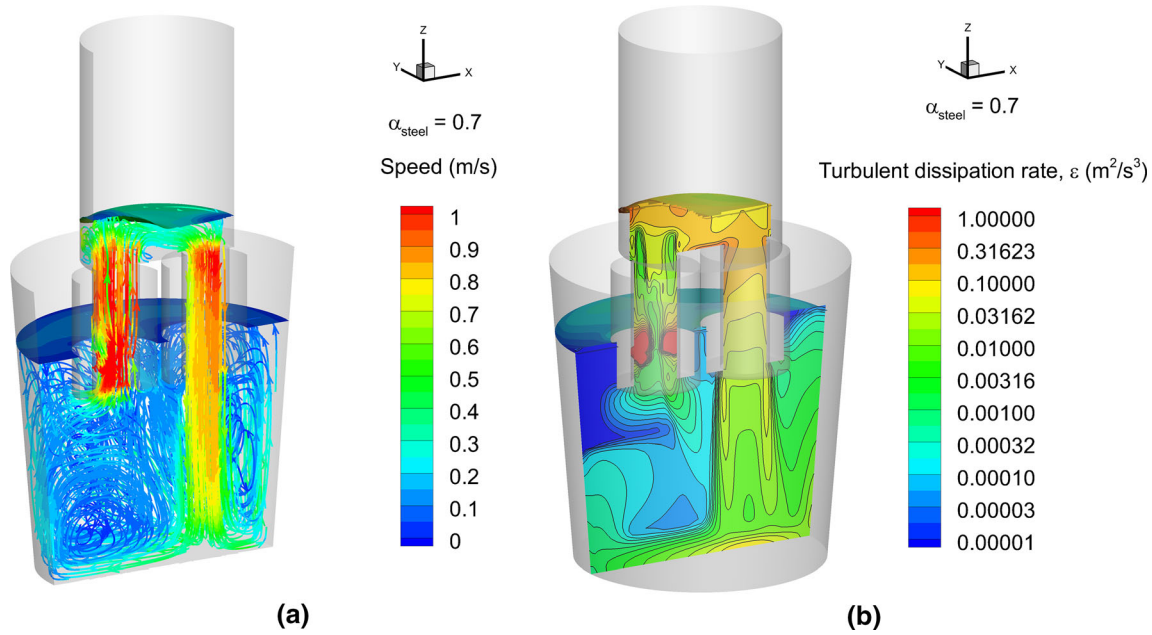


Fig. 2—Three-dimensional velocity and turbulent feature distribution of molten steel-argon system ( $N = 12$ ,  $G = 3000$  NL/min,  $P_{vacuum} = 100$  Pa): (a) velocity; (b) turbulent kinetic dissipation rate.

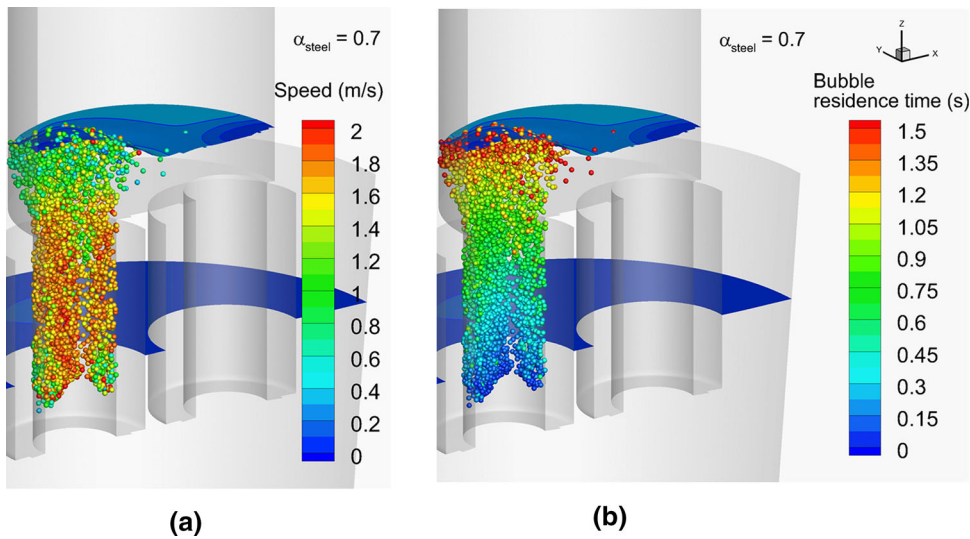


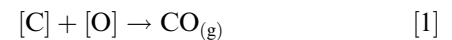
Fig. 3—Velocity and residence time distribution of bubbles: (a) velocity; (b) residence time.

injection from the up-leg snorkel to the surface of molten steel in the vacuum chamber. The average residence time of bubbles from blowing to moving to the surface of molten steel in the vacuum chamber is about 1.5 seconds.

### III. DECARBURIZATION OF THE MOLTEN STEEL DURING RH REFINING PROCESS

#### A. Formulation of the Decarburization

The basic equation of decarburization reaction of molten steel<sup>[24]</sup> was:



$$\Delta G_r^\ominus = -22364 - 39.63T = -RT \ln K \quad [2]$$

The equilibrium constant at 1873 K can be calculated by,

$$K_{1873K} = \frac{P_{CO}/P^\ominus}{a_{[C]}a_{[O]}} = \frac{P_{CO}/P^\ominus}{f_{[C]}f_{[O]}[\text{pct C}]_e[\text{pct O}]_e} \quad [3]$$

where,  $P_{CO}$  is the partial pressure of CO gas, Pa;  $P^\ominus$  is the standard atmospheric pressure, Pa; [pct C] and [Pct O] are the mass concentration of dissolved carbon

**Table III. Activity Interaction Coefficients of Elements in Molten Steel<sup>[24–26]</sup>**

$e_i^j$	C	O	Al	Si	Mn
C	0.142	-0.34	0.043	0.078	-0.012
O	-0.45	-0.2	-3.85	-0.131	-0.021

and dissolved oxygen at reaction interface respectively, wt pct;  $f_{[C]}$  and  $f_{[O]}$  are the activity coefficients of carbon and oxygen in the molten steel respectively, and the formulas are as follows:

$$\lg f_{[C]} = e_C^C [\text{pct C}] + e_C^O [\text{pct O}] + \sum_j e_C^j [\text{pct } j] \quad [4]$$

$$\lg f_{[O]} = e_O^C [\text{pct C}] + e_O^O [\text{pct O}] + \sum_j e_O^j [\text{pct } j] \quad [5]$$

where,  $e_i^j$  is the activity interaction coefficient. In this study, the effects of carbon, oxygen, aluminum, silicon and manganese on the activity coefficients of carbon and oxygen in molten steel are considered. In the calculation of decarburization reaction, the content of carbon and oxygen in molten steel will change with time. It is considered that the composition of other elements remains unchanged. According to the changes of carbon and oxygen in molten steel, the activities of carbon and oxygen are calculated using the current carbon and oxygen content. But the influence of other components on the activities of carbon and oxygen is excluded. The activity interaction coefficient used in the calculation is shown in Table III.

According to the molecular weight, for every 3 kg of carbon consumed, 4 kg of oxygen is consumed, as follows.

$$-\frac{d[\text{pct C}]}{dt} = K_C ([\text{pct C}] - [\text{pct C}]_e) \quad [6]$$

$$-\frac{d[\text{pct O}]}{dt} = \frac{4}{3} \times \frac{d[\text{pct C}]}{dt} = K_O ([\text{pct O}] - [\text{pct O}]_e) \quad [7]$$

where,  $-\frac{d[\text{pct C}]}{dt}$  and  $-\frac{d[\text{pct O}]}{dt}$  are the reaction rates of [C] and [O] in the molten steel respectively, wt pct/s;  $K_C$  and  $K_O$  are the apparent rate constants,  $s^{-1}$ ;  $[\text{pct C}]_e$  and  $[\text{pct O}]_e$  are the equilibrium [C] and [O] contents, wt pct.

The above equation assumes that the chemical reaction is not the controlling step, and the relationship between equilibrium [C] and [O] concentration could be derived as follows<sup>[19]</sup>:

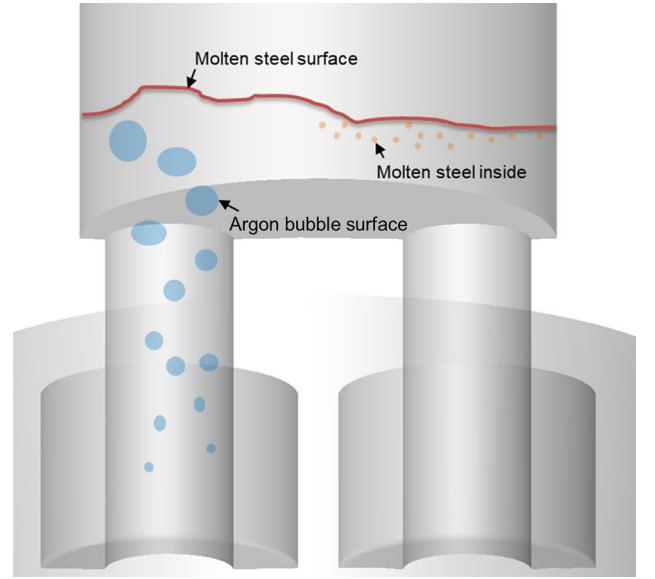


Fig. 4—Schematic diagram of decarburization reaction in RH refining process.

$$K_C ([\text{pct C}] - [\text{pct C}]_e) = \frac{3}{4} K_O ([\text{pct O}] - [\text{pct O}]_e) \quad [8]$$

$$[\text{pct C}]_e \cdot [\text{pct O}]_e = \frac{P_{CO}/P^\ominus}{K \cdot f_{[C]} f_{[O]}} \quad [9]$$

$$[\text{pct C}]_e = \frac{K_O}{2} \left( \frac{[\text{pct C}] - 3[\text{pct O}]}{K_O} - \frac{3[\text{pct O}]}{4K_C} \right) + \left( \left( \frac{3[\text{pct O}]}{4K_C} - \frac{[\text{pct C}]}{K_O} \right)^2 + \frac{3P_{CO}}{f_{[C]} f_{[O]} K_{1873K} K_C K_O} \right)^{0.5} \quad [10]$$

$$[\text{pct O}]_e = \frac{2K_C}{3} \left( \frac{3[\text{pct O}]}{4K_C} - \frac{[\text{pct C}]}{K_O} \right) + \left( \left( \frac{3[\text{pct O}]}{4K_C} - \frac{[\text{pct C}]}{K_O} \right)^2 + \frac{3P_{CO}}{f_{[C]} f_{[O]} K_{1873K} K_C K_O} \right)^{0.5} \quad [11]$$

### B. Three Decarburization Reaction Sites

Decarburization reaction in the RH refining process mainly occurs on three sites: inside of molten pool (interface between CO bubble and molten steel), surface of molten pool in vacuum chamber and surface of argon bubble in circulating gas, as shown in Figure 4.

### 1. Interior of the molten steel

When the equilibrium partial pressure of CO,  $P_{CO}^e$ , corresponding to the [C] and [O] content in the molten steel is greater than the sum of the static pressure  $P_{local}$  and the pressure  $P_{critical}$ , the decarburization reaction can occur,

$$P_{CO}^e > P_{local} + P_{critical} \quad [12]$$

$$P_{critical} = \frac{2\sigma_{gl}}{r_{CO}} \quad [13]$$

where,  $\sigma_{gl}$  is the interfacial tension between generated CO bubbles and the molten steel, N/m;  $r_{CO}$  is the radius of the generated CO bubble, m. In previous studies,<sup>[14,27]</sup> when the value of  $P_{critical}$  is 0.02 atm, the calculated values are in good agreement with the experimental values.

According to the proportion of [C] and [O], the restrictive step is determined. The critical [C] and [O] ratio calculation formula<sup>[16]</sup> is as follows:

$$\left(\frac{[C]}{[O]}\right)_{Cr} = \frac{M_C K_{O,interior}}{M_O K_{C,interior}} = \frac{M_C 1/Q + 1/A_{interior}k_{C,interior}}{M_O 1/Q + 1/A_{interior}k_{O,interior}} \quad [14]$$

where,  $M_C$  and  $M_O$  are the molar mass of carbon and oxygen, 12 and 16 g/mol, respectively;  $Q$  is the volume circulation flow of the molten steel, m<sup>3</sup>/s; which is calculated according to the longitudinal velocity and the cross-sectional area of the down-leg snorkel,  $Q = A_{down} \cdot \bar{u}_{down} = \pi \times 0.325^2 \times 0.71 = 0.235$  m<sup>3</sup>/s;  $A_{interior}k_{C,interior}$  and  $A_{interior}k_{O,interior}$  are volumetric mass transfer coefficients of carbon and oxygen in the molten steel, m<sup>3</sup>/s;  $k_{C,interior}$  and  $k_{O,interior}$  are the mass transfer coefficients of carbon and oxygen in the molten steel, m/s. The volumetric mass transfer coefficients were related to the flow field, which was calculated during the simulation process and changed with calculation time.

When the mass transfer of [C] is the restrictive step:

$$K_{C,interior} = \frac{QA_{interior}k_{C,interior}}{V_{interior}(A_{interior}k_{C,interior} + Q)} \quad [15]$$

$$K_{O,interior} = \frac{M_O [C]}{M_C [O]} \quad [16]$$

$$K_{C,interior} = \frac{M_O [C]}{M_C [O]} \frac{QA_{interior}k_{C,interior}}{V_{interior}(A_{interior}k_{C,interior} + Q)}$$

When the mass transfer of [O] is the restrictive step:

$$K_{O,interior} = \frac{QA_{interior}k_{O,interior}}{V_{interior}(A_{interior}k_{O,interior} + Q)} \quad [17]$$

$$K_{C,interior} = \frac{M_C [O]}{M_O [C]} \quad [18]$$

$$K_{O,interior} = \frac{M_C [O]}{M_O [C]} \frac{QA_{interior}k_{C,interior}}{V_{interior}(A_{interior}k_{C,interior} + Q)}$$

where,  $V_{interior}$  is the volume of the molten steel in which internal decarburization occurs, m<sup>3</sup>. The mass transfer coefficients of carbon and oxygen in the molten steel are calculated by the formula<sup>[5,16]</sup>:

$$k_{C,interior} = (\varepsilon \times 1000)^{1.5} \quad [19]$$

$$k_{O,interior} = 0.69 \times k_{C,interior} \quad [20]$$

### 2. Free surface of the molten steel in the vacuum chamber

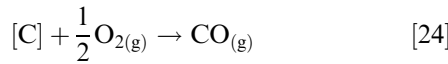
In order to meet the composition requirements of ultra-low carbon steel, the decarburization reaction was accelerated by blowing oxygen<sup>[11]</sup> in the vacuum chamber during the RH refining process. After oxygen is blown into the steel liquid surface of the vacuum chamber, oxygen dissolves into the steel liquid. The Reaction Eq. [28] is as follows:



$$\Delta G_{sol}^{\ominus} = -117150 - 2.89T = -RT \ln K \quad [22]$$

$$K_{1873K} = \frac{[pct O]f_{[O]}}{(P_{O_2}/P^{\ominus})^{1/2}} \quad [23]$$

However, the existence of carbon in molten steel will limit the dissolution of oxygen in the molten steel. Under a certain temperature and pressure, the product of carbon and oxygen is constant. Therefore, it is necessary to calculate the dissolved oxygen content of molten steel according to the carbon content on the surface of molten steel. When the carbon content in the molten steel is high, oxygen is difficult to dissolve into the molten steel, but reacts with the carbon in the molten steel. The Eq. [24], which is the sum of the above Reaction Eqs. [1] and [21].



$$\Delta G_r^\ominus = -139514 - 42.52T = -RT \ln K \quad [25]$$

$$K_{1873\text{K}} = \frac{P_{\text{CO,surface}}/P^\ominus}{(P_{\text{O}_2}/P^\ominus)^{1/2}[\text{pct C}]f_{[\text{C}]}} \quad [26]$$

$$P_{\text{O}_2} = \frac{n_{\text{O}_2}^s}{n_{\text{Ar}}^s + n_{\text{O}_2}^s} P_{\text{vacuum}} \quad [27]$$

$$P_{\text{CO,surface}} \approx P_{\text{vacuum}} \quad [28]$$

When there is oxygen blowing in the vacuum chamber, assuming that the controlling step of the carbon–oxygen reaction at the gas–liquid interface in the vacuum chamber is the mass transfer of carbon, the equilibrium carbon content,  $[\text{pct C}]_e$ , at the phase interface in the vacuum chamber is calculated according to formula [26], and then the equilibrium oxygen content,  $[\text{pct O}]_e$ , at the phase interface is calculated according to formula [3]. The apparent decarburization reaction rate and oxygen dissolution rate at the phase interface of the vacuum chamber are as follows:

$$-\frac{d[\text{Pct C}]}{dt} = K_{\text{C,surface}} \left( [\text{Pct C}] - [\text{Pct C}]_{e,\text{surface}} \right) \quad [29]$$

$$-\frac{d[\text{pct O}]_{\text{blowing}}}{dt} = K_{\text{O,blowing}} \left( [\text{pct O}] - [\text{pct O}]_{e,\text{surface}} \right) \quad [30]$$

$$K_{\text{C,surface}} = \frac{A_{\text{surface}} k_{\text{C,surface}}}{V_{\text{surface}}} \quad [31]$$

where,  $k_{\text{C,surface}}$  is the mass transfer coefficient of carbon on the free surface of the molten steel in the vacuum chamber, and the value in the calculation is  $0.005 \text{ m/s}^{[17]}$ ;  $A_{\text{surface}}$  is the area of the gas–liquid interface in the vacuum chamber,  $\text{m}^2$ ;  $V_{\text{surface}}$  is the volume of the molten steel occurring surface decarburization reaction,  $\text{m}^3$ .

A certain oxygen blowing period is set in the model, the reaction on the surface of molten steel in the vacuum chamber is Eq. [24] when oxygen blowing, and Eq. [1] when no oxygen blowing. The equilibrium carbon content at the interface calculated by the two methods is different, and there is no oxygen dissolution reaction on the surface of molten steel in the vacuum chamber when no oxygen blowing. No matter whether oxygen blowing or not, the reaction in the molten steel and on the surface of argon bubbles is the Reaction Eq. [1].

It should be pointed out that oxygen blowing into the top of the vacuum chamber will affect the flow of molten steel in the vacuum chamber, but this study ignored the effect of oxygen blowing on the flow field of the molten steel, and only considered the dissolution and diffusion of oxygen on the surface of the molten steel in the vacuum chamber.

### 3. Argon bubbles surface

The apparent rate constant of decarburization reaction on the surface of argon bubble,  $K_{\text{C,bubble}}$ , is expressed as:

$$K_{\text{C,bubble}} = \frac{A_{\text{bubble}} k_{\text{C,bubble}}}{V_{\text{bubble}}} \quad [32]$$

$$k_{\text{C,bubble}} = 2 \left( \frac{D_{\text{C}}}{\pi t_e} \right)^{0.5} \quad [33]$$

$$t_e = \frac{d_b}{u_R} \quad [34]$$

$$u_R = u_b - u_l \quad [35]$$

where,  $A_{\text{bubble}}$  is the contact area between argon bubble and the molten steel,  $\text{m}^2$ ;  $D_{\text{C}}$  is the diffusion coefficient of  $[\text{C}]$  in the molten steel, which is  $2.24 \times 10^{-8} \text{ m}^2/\text{s}^{[29,30]}$ ;  $t_e$  is the contact time, s;  $d_b$  is the diameter of argon bubble, m;  $u_R$  is the relative velocity between the argon bubble and the molten steel, m/s.

$$K_{\text{O,bubble}} = \frac{A_{\text{bubble}} k_{\text{O,bubble}}}{V} \quad [36]$$

$$k_{\text{O,bubble}} = 2 \left( \frac{D_{\text{O}}}{\pi t_e} \right)^{0.5} \quad [37]$$

where,  $D_{\text{O}}$  is the diffusion coefficient of  $[\text{O}]$  in the molten steel, which is  $1.26 \times 10^{-8} \text{ m}^2/\text{s}^{[29,30]}$

According to the proportion of  $[\text{C}]$  and  $[\text{O}]$ , the restrictive step is determined, in which the critical  $[\text{C}]$  and  $[\text{O}]$  ratio calculation formula<sup>[16]</sup> is as follows:

$$\left( \frac{[\text{C}]}{[\text{O}]} \right)_{\text{Critical}} = \frac{M_{\text{C}} K_{\text{O,bubble}}}{M_{\text{O}} K_{\text{C,bubble}}} \quad [38]$$

When the mass transfer of  $[\text{C}]$  is a limiting step,  $K_{\text{O,bubble}}$  is calculated according to the  $K_{\text{C,bubble}}$  calculated by formula [32]:

$$K_{\text{O,bubble}} = \frac{4}{3} K_{\text{C,bubble}} \quad [39]$$

When the mass transfer of  $[\text{O}]$  is a limiting step,  $K_{\text{C,bubble}}$  is calculated according to the  $K_{\text{O,bubble}}$  calculated by formula [36]:

**Table IV. Key Parameters in the Decarburization Model**

Zones	Interior of Molten Steel	Argon Bubbles Surface	Free Surface in Vacuum Chamber
$k_C$ (m/s)	$(\varepsilon \times 1000)^{1.5}$	$2\left(\frac{D_C}{\pi r_c}\right)^{0.5}$	0.005
$k_O$ (m/s)	$0.69 \times k_C$	$2\left(\frac{D_O}{\pi r_c}\right)^{0.5}$	—
Judgment	judging the restrictive step according		assuming carbon transportation is the controlling step
	$\left(\frac{[C]}{[O]}\right)_{\text{Critical}} = \frac{M_C K_O}{M_O K_C}$		

$$K_{C,\text{bubble}} = \frac{3}{4} K_{O,\text{bubble}} \quad [40]$$

In practice, the CO partial pressure of the decarburization reaction on the surface of argon bubbles is the ratio of the molar amount of CO generated to the total molar amount of argon bubbles:

$$P_{CO,\text{bubble}} = \frac{n_{CO}^b}{n_{Ar}^b + n_{CO}^b} P_{\text{Bubble,local}} \quad [41]$$

where  $P_{CO,\text{Bubble}}$  is the partial pressure of CO generated on the surface of argon bubble, Pa;  $P_{\text{Bubble,local}}$  is the static pressure of argon bubble, Pa;  $n_{CO}^b$  is the molar amount of CO generated on the surface of argon bubble, mol;  $n_{Ar}^b$  is the molar amount of argon in the argon bubble, mol. Considering the current work is based on a steady-state (shown in Figures 2 and 3), and bubbles residence time is about 1.5 seconds, which is short. Thus, the  $P_{CO,\text{bubble}}$  was assumed to be zero, meaning the bubble is a vacuum for the formed CO gas produced by carbon and oxygen reaction.

To summarized, some key parameters are listed in Table IV.

### C. Decarburization Model Coupling with Fluid Flow

According to the reaction conditions in different reaction regions, the reaction rates corresponding to different positions are calculated firstly, and then the decarburization reaction is coupled with fluid flow, and finally the spatial distribution of carbon and oxygen concentration in molten steel is predicted.

The variation of carbon and oxygen concentration in the molten steel during RH refining is solved by the concentration equation of carbon and oxygen:

$$\frac{\partial}{\partial t}(\rho[C]) + \nabla \cdot (\rho \vec{u}[C]) = \nabla \cdot \left( \left( \frac{\mu_t}{Sc_t} + \rho D_{[C]} \right) \nabla [C] \right) + S_{[C]} \quad [42]$$

$$\frac{\partial}{\partial t}(\rho[O]) + \nabla \cdot (\rho \vec{u}[O]) = \nabla \cdot \left( \left( \frac{\mu_t}{Sc_t} + \rho D_{[O]} \right) \nabla [O] \right) + S_{[O]} \quad [43]$$

where [C] and [O] are the mass percent contents of carbon and oxygen in molten steel, wt pct.  $S_{[C]}$  and  $S_{[O]}$  are the reaction source terms of the mass concentration changes of carbon and oxygen caused by

decarburization reaction and the mass concentration changes of oxygen caused by the oxygen blowing process:

$$S_{[C]} = -\rho_1 K_C ([\text{pct C}] - [\text{pct C}]_e) \quad [44]$$

$$S_{[O]} = \frac{4}{3} S_{[C]} + \frac{d[\text{pct O}]_{\text{blowing}}}{dt} \quad [45]$$

Based on the obtained three-dimensional flow field, the mechanism and transport model of decarburization reaction are added to the calculation by User-defined Functions (UDF), and the concentration fields of carbon and oxygen in three-dimensional flow space are solved.

### D. Calculation Conditions and Process

The initial carbon and oxygen contents in the molten steel are 300 and 600 ppm, respectively. The distribution of carbon and oxygen content is uniform in the molten steel. The boundary condition on the walls of the RH reactor is the fluxes of the carbon and oxygen contents are zero, meaning the wall has no effect on the carbon and oxygen variation. The computational iteration process is shown in Figure 5. For each cell, the input parameters are the local carbon content, local oxygen content, and fluid features, and then the reaction zone was judged, corresponding mechanism was employed to calculate  $k_C$ ,  $k_O$ ,  $P_{CO}$ ,  $K_C$ ,  $K_O$ ,  $S_{[C]}$ , and  $S_{[O]}$ , sequentially. The obtained decarburization rate was coupled with the flow field, based on it, the carbon and oxygen content was updated in each iteration time step, and the new carbon and oxygen content was used as the input parameter of the next time step. The calculation time step is 0.1 seconds, and the total calculation time is 1200 seconds.

## IV. RESULTS OF THE DECARBURIZATION MODEL CALCULATION

### A. Model Validation

Limited by the extremely difficult sampling on each reaction zones in the vacuum chamber, the verification process comes from the comparison of carbon content between the sampling in the ladle and a monitoring point in the calculation, as shown in Figure 6. The

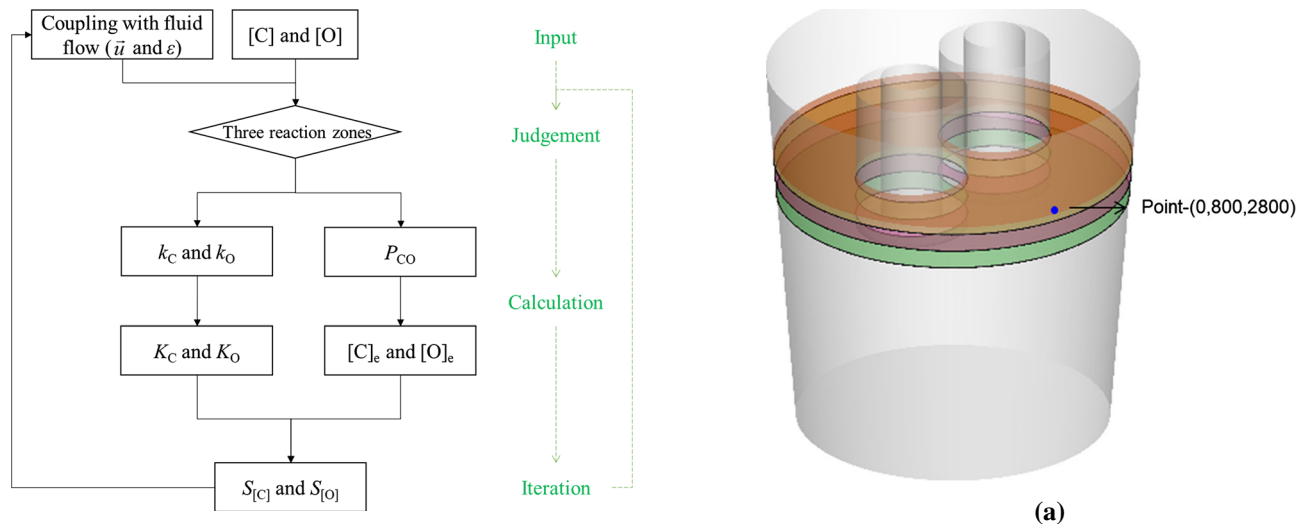


Fig. 5—Calculation flow chart of the current decarburization model.

monitor is located between the snorkels and the ladle wall in the RH ladle at 300 mm below the steel liquid level, corresponding to the sampling position of the industrial test. The specific position is shown in Figure 6(a). The calculation condition is that the argon gas flow rate is 3000 NL/min, oxygen blowing operation is carried out in 0 to 3 minutes, and the oxygen blowing flow rate is 1200 Nm<sup>3</sup>/h. Figure 6(b) shows the comparison of the variation of the predicted and measured carbon content. At the beginning of the calculation, there is a short platform period for [C] content in molten steel. This is because the decarburization reaction mainly occurs in the RH vacuum chamber, and the monitor is set in the ladle, so it takes some time to complete [C] transmission. The decarburization reaction is faster in the early stage; at about 5 minutes, the [C] content in molten steel decreased from 300 to 70 ppm; then, with the decrease of [C] and [O] content in molten steel, the decarburization rate also decreases. The simulation results are in good agreement with the industrial test results, which indicates that the current decarburization reaction model can simulate the decarburization process of molten steel in the actual RH vacuum refining process.

### B. Carbon and Oxygen Transport

Figures 7 and 8 show the contour of [C] and [O] concentration variation with time on the central section of RH. All results shown in this chapter do not consider the oxygen blowing. It can be seen that the decrease of [C] concentration first occurs in the vacuum chamber, and then the carbon content in the whole ladle gradually decreases with the progress of decarburization reaction and the transport of carbon with the molten steel flow and concentration difference. At 600 seconds, the [C] content in the ladle has reached a low level. Finally, with the decarburization reaction, the [C] and [O] in molten steel have reached a plateau, and the concentration difference between vacuum chamber and ladle has become negligible.

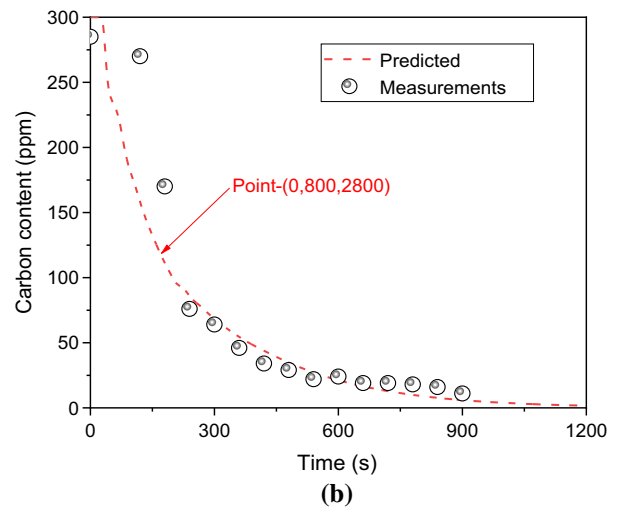
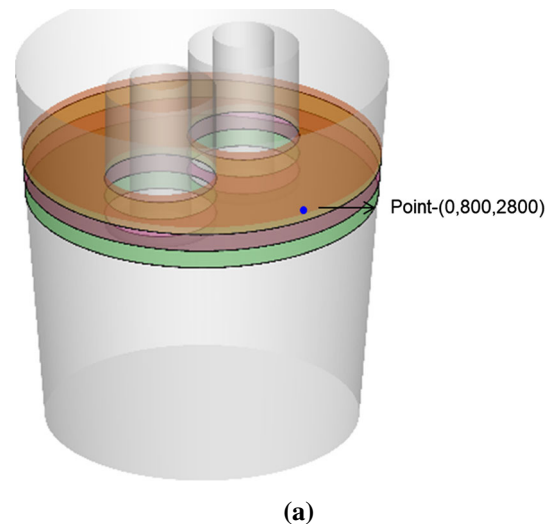


Fig. 6—Comparison of carbon content variation at monitor between numerical calculation and industrial measurements: (a) monitor position; (b) validation.

Figure 9 shows the decarburization reaction rate in the central section and gas–liquid interface ( $\alpha_1 = 0.9$ ). The decarburization reaction mainly occurs on the surface of the argon bubbles in the up-leg snorkel, inside the molten pool and the surface of the molten steel in the vacuum chamber. In addition, when the reaction rate of decarburization in molten steel decreases, the reaction volume also decreases, which is due to the decrease of [C] content in molten steel caused by decarburization.

To increase the decarburization rate, more attention should be paid to the vacuum chamber, such as increasing the contact area between the molten steel and the vacuum environment in the vacuum chamber, and strengthen the stirring to enhance the transport of carbon and oxygen. Compared with the molten steel surface and argon bubble surface in the vacuum chamber, the whole reaction area in the molten pool is larger, especially in the corresponding area of the up-leg snorkel in the vacuum chamber. Since the

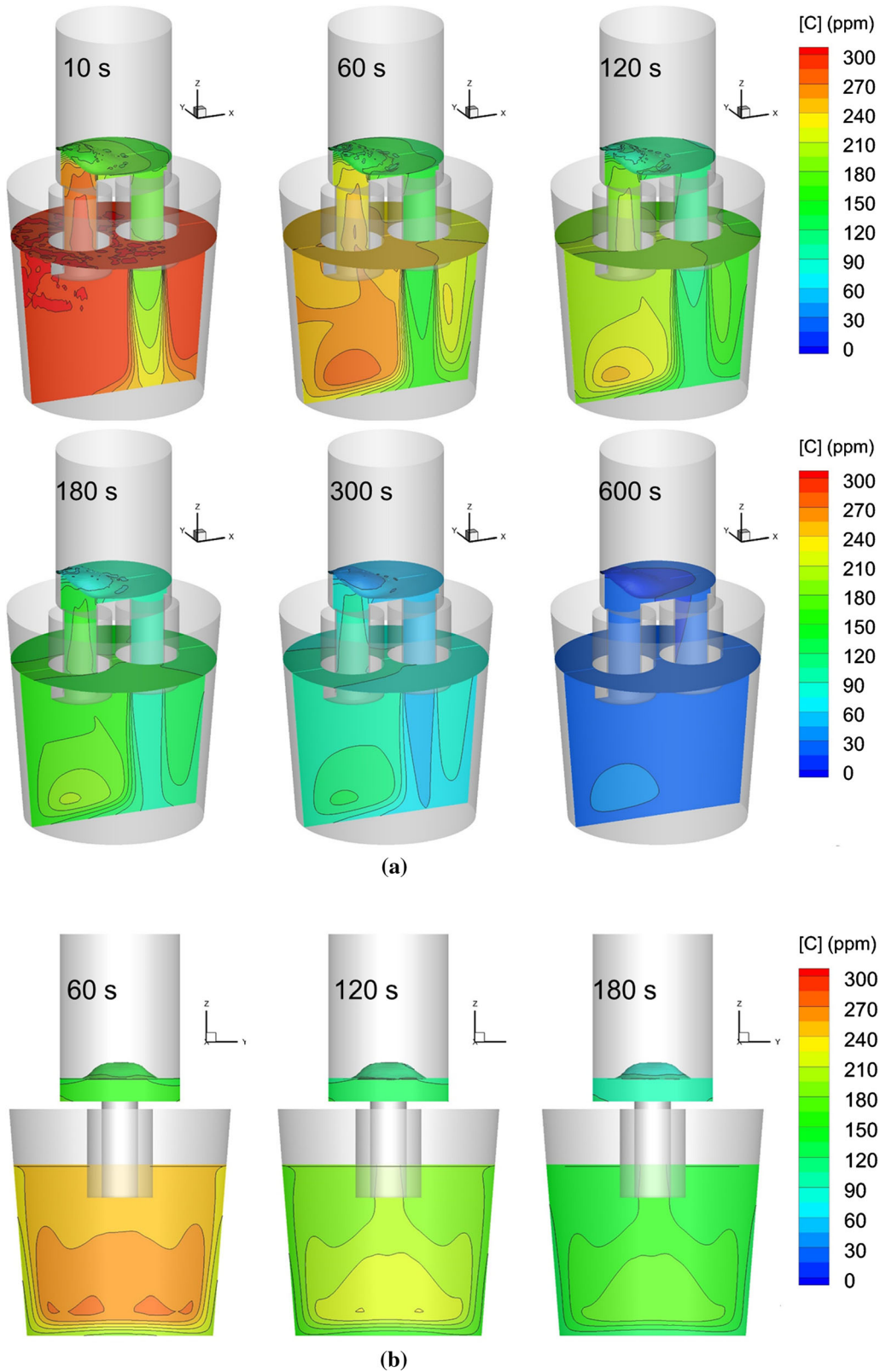


Fig. 7—Distribution of [C] concentration in the molten steel on the central plane and the surface in vacuum chamber: (a) passing through the snorkels; (b) normal to the connecting line of two snorkels.

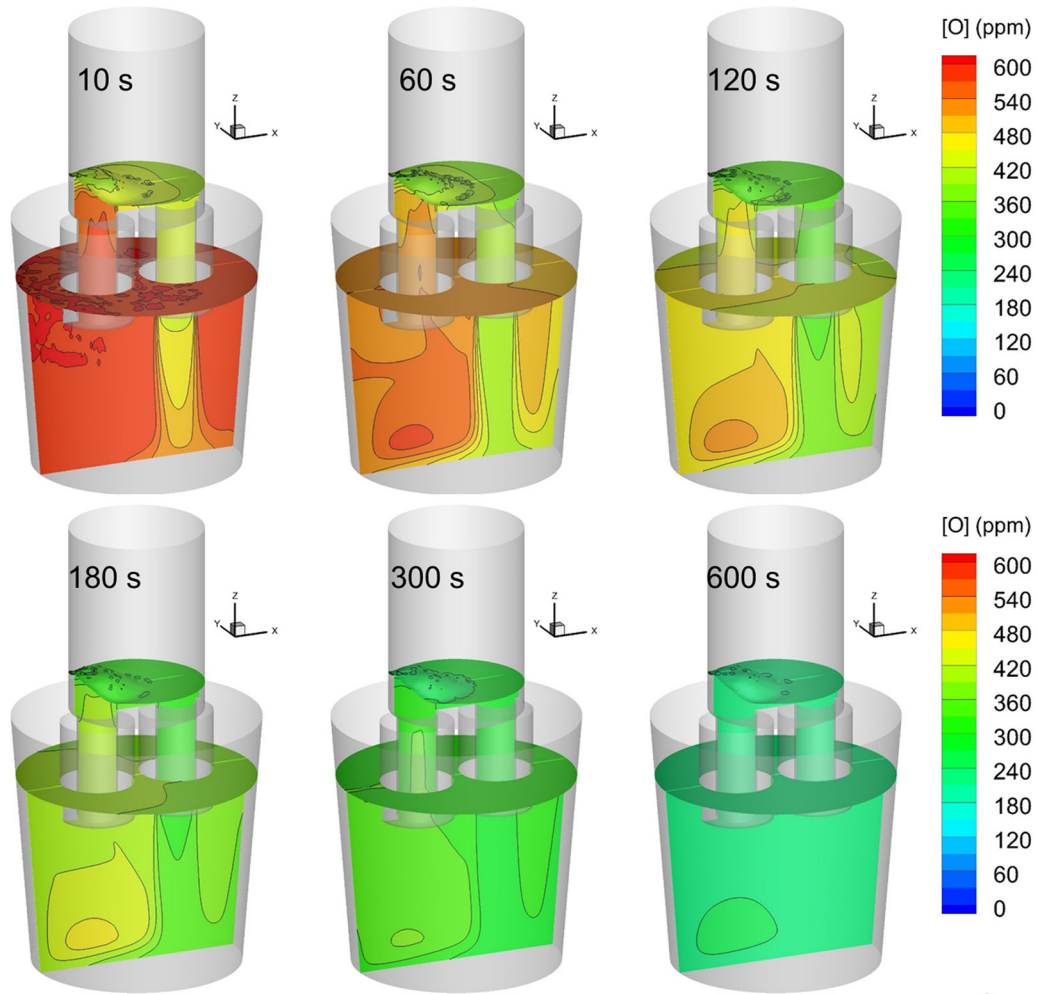


Fig. 8—Distribution of [O] concentration in the molten steel on the central plane passing through the snorkels and the surface in vacuum chamber.

decarburization reaction only takes place in the vacuum chamber and up-leg snorkel, that increasing the RH circulation flow rate makes the molten steel flow to drive the transport of [C] and [O] is also important to improve the decarburization efficiency.

According to the carbon content difference in each cell between the current time step and the previous time step, the apparent decarburization rate is obtained by the formula [46].

$$\frac{d[C]_{\text{apparent}}}{dt} = -\frac{[C]_{i,t} - [C]_{i,t-1}}{\Delta t} \quad [46]$$

The apparent decarburization reaction rate of molten steel in RH at different times is shown in Figure 10. The results of 10 to 60 seconds in the figure correspond to the legend on the upper, and the results of 120 to 600 seconds correspond to the legend on the lower. In the first 60 seconds, the molten steel with low [C] content in the vacuum chamber flows into the ladle from the vacuum chamber, and then gradually flows and diffuses to the ladle wall, which is consistent with the flow cycle of molten steel, and finally leads to the apparent

decarburization effect of reducing [C] content in the ladle. At the beginning of the reaction, the apparent decarburization rate of the molten steel flowing into the ladle from the down-leg snorkel is higher, because the decarburization rate of the vacuum chamber is faster at the beginning stage, the carbon content in the molten steel decreases faster, while the molten steel with lower carbon content flows into the ladle through the down-leg snorkel following the fluid flow, leading the apparent decarburization rate of molten steel at the outlet of the down-leg snorkel is higher. After 120 seconds, the apparent decarburization rate decreased by about an order of magnitude, and the distribution of [C] content in the whole RH vacuum chamber and ladle tended to be uniform, which is introduced by the flow and diffusion. The real decarburization reaction mainly occurs in the up-leg snorkel and the vacuum chamber, and the volume of molten steel in the vacuum chamber accounts for less than 10 pct of the total volume of molten steel, therefore the molten steel transfer between the vacuum chamber and the ladle will directly affect the decarburization reaction rate of the whole molten steel.

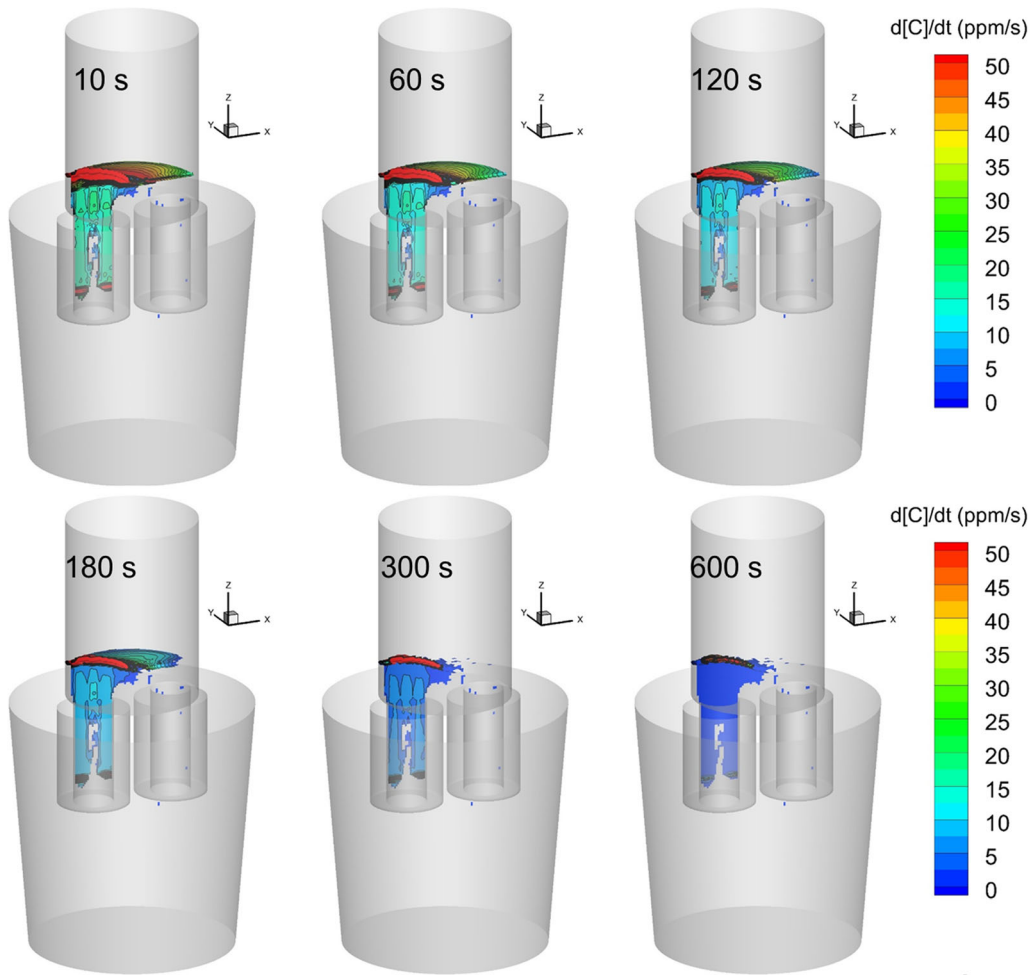


Fig. 9—Transient three-dimensional distribution of decarburization reaction rate in the molten steel at different time during RH refining process.

The real chemical reaction mainly occurs in the vacuum chamber, and with the fluid flow and mass transfer process, the carbon content in the whole molten steel decreases uniformly.

### C. Effect of Oxygen Blowing on Decarburization Rate

To study the influence of the top oxygen supply system on the RH decarburization reaction, four conditions of oxygen supply were compared: no oxygen blowing, oxygen blowing at the beginning of decarburization, oxygen supply after 3 and 5 minutes decarburization.

Figure 11 shows the variation of the carbon content in the molten steel at the monitor (point-(0, 800 mm, 2800 mm)) under four oxygen supply conditions. It can be seen that no matter when oxygen blowing, oxygen blowing operation can promote the decarburization process of RH refining.

To compare the contribution of three decarburization sites to total decarburization, the percentage of decarburization accumulated in the total amount of the three reaction sites was compared, as shown in Figure 12. The internal reaction of molten steel contributes the most to

the decarburization, accounting for about 55.9 pct of the total. The argon bubble surface and the free surface of the vacuum chamber contribute 32.5 and 11.6 pct, respectively.

The results show that the proportion of decarburization reaction on the surface of the molten steel in the vacuum chamber increases when the oxygen supply operation was employed. Accordingly, the proportion of the reaction inside the molten steel in the vacuum chamber and the decarburization reaction on the surface of the argon bubble in the up-leg is slightly reduced. With the postponing of the oxygen supply beginning time, the proportion of decarburization on the surface of vacuum chamber steel decreases gradually. When the oxygen supply at the beginning of the decarburization, the contribution of the free surface of the molten steel in the vacuum chamber increased from 11.6 to 28.3 pct. The promoting effect of oxygen blowing on the decarburization process is more obvious when the carbon content is relatively high. When the carbon content is very low, the transportation of the carbon in the molten steel is the restricted step in the decarburization reaction. Thus, the earlier starting blow oxygen, the more intense the decarburization reaction

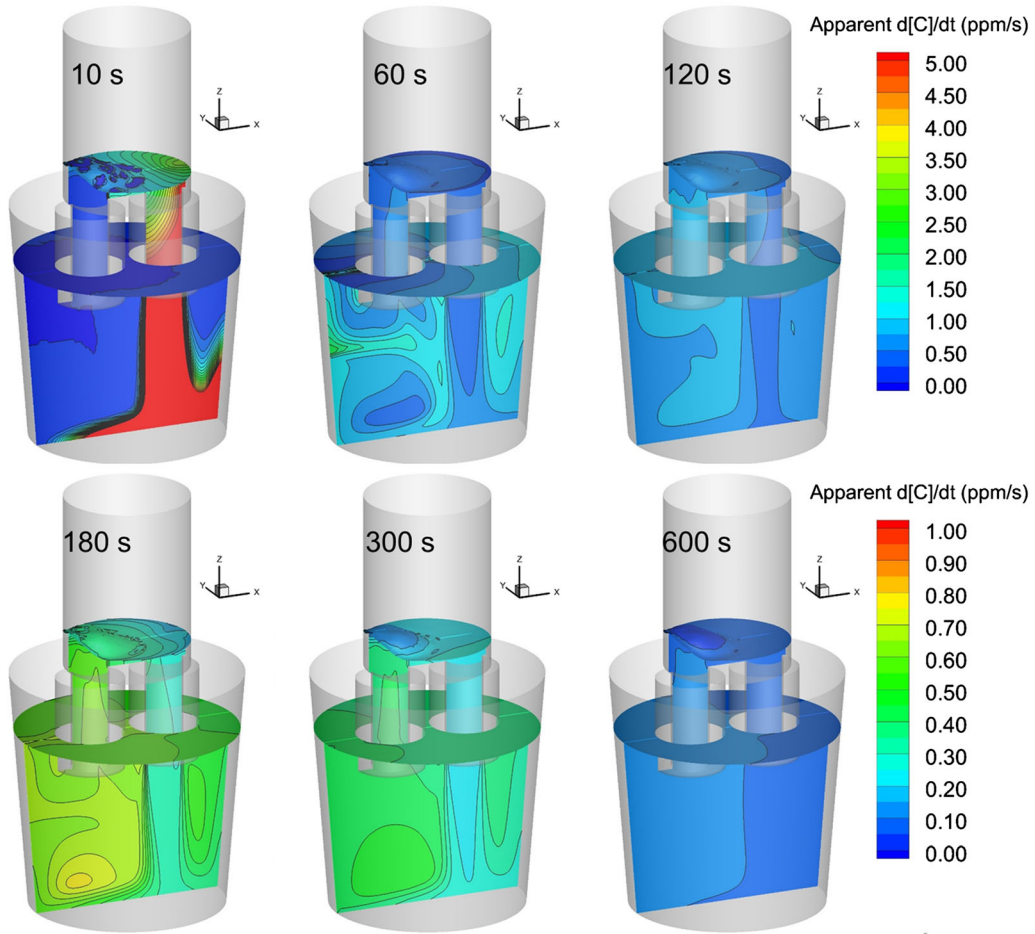


Fig. 10—Three-dimensional distribution of apparent decarburization rate in the molten steel at different time.

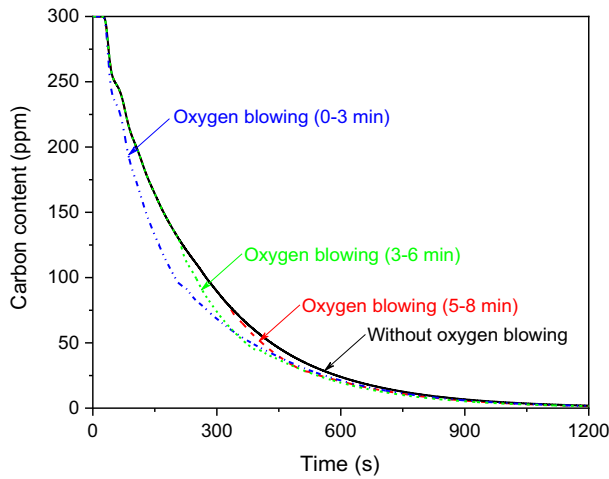


Fig. 11—Variation of carbon content of monitors in the molten steel with time under different oxygen supply conditions.

on the surface. When the carbon content in the molten steel is high, the oxygen blowing operation can significantly promote the decarburization reaction. When the carbon content in the molten steel is low, improving the

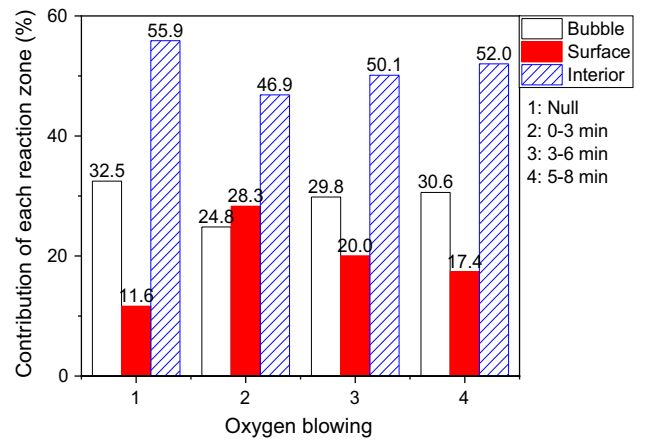


Fig. 12—Contribution of each reaction zone on decarburization under different oxygen supply conditions.

circulation flow rate of the molten steel is more conducive to the further reduction of the carbon content in the molten steel in the ladle of the RH.

## V. CONCLUSIONS

In the current study, the decarburization reaction in the RH vacuum refining process was simulated. The oxygen dissolution from the surface of molten steel in the vacuum chamber was considered. The variation of [C] concentration in the RH reactor and the decarburization reaction rate in each region were obtained.

- (1) In the case of without oxygen blowing, the decarburization reaction inside of the molten steel in the vacuum chamber has the largest contribution to the overall decarburization amount, accounting for 55.9 pct, while the proportion of the argon bubble surface and the molten steel free surface in the vacuum chamber are 32.5 and 11.6 pct, respectively.
- (2) The decarburization reaction mainly occurs in the RH vacuum chamber, and fluid flow and mass transfer drive the reduction of carbon content in RH ladle, so as to reduce the carbon content in molten steel in the Whole RH reactor.
- (3) No matter when oxygen blowing, this operation can promote the decarburization process of RH refining. The increase of oxygen supply operation leads to the increase of the proportion of decarburization reaction on the surface of molten steel in the vacuum chamber, which can increase the percentage of decarburization reaction on the surface of molten steel in the vacuum chamber from 11.6 to 28.3 pct.
- (4) When the carbon content in the molten steel is high, the oxygen blowing operation can significantly promote the decarburization reaction. When the carbon content in the molten steel is low, improving the circulation flow rate of the molten steel is more conducive to the further reduction of the carbon content in the molten steel in the ladle of the RH.

## ACKNOWLEDGMENTS

The authors are grateful for support from the National Natural Science Foundation of China (Grant No. U1860206, No. 51725402), the Fundamental Research Funds for the Central Universities (Grant No. FRF-BD-20-04A), the High Steel Center (HSC) at Yanshan University, Beijing International Center of Advanced and Intelligent Manufacturing of High Quality Steel Materials (ICSM), the High Quality Steel Consortium (HQSC) of University of Science and Technology Beijing, China.

## CONFLICT OF INTEREST

On behalf of all authors, the corresponding author states that there is no conflict of interest.

## NOMENCLATURE

$a_{[C]}$  Carbon activity in molten steel (wt pct)  
 $a_{[O]}$  Oxygen activity in molten steel (wt pct)

$A$	Reaction area ( $m^2$ )
$A_S$	Area of decarburization reaction on the surface of vacuum chamber ( $m^2$ )
$Ak_C$	Volumetric mass transfer coefficient of carbon ( $m^3/s$ )
$Ak_O$	Volumetric mass transfer coefficient of oxygen ( $m^3/s$ )
$d_b$	Bubble diameter (m)
$D_C$	Diffusion coefficient of carbon ( $m^2/s$ )
$D_O$	Diffusion coefficient of oxygen ( $m^2/s$ )
$e_i^j$	Activity interaction coefficient
$f_{[C]}$	Activity coefficient of [C]
$f_{[O]}$	Activity coefficient of [O]
$G$	Flow rate of lifting gas (NL/min)
$\Delta G^\ominus$	Gibbs free energy (J/mol)
$k_C$	Mass transfer coefficient of carbon (m/s)
$k_O$	Mass transfer coefficient of oxygen (m/s)
$K$	Equilibrium constant of carbon oxygen reaction
$K_C$	Decarburization reaction rate constant ( $s^{-1}$ )
$K_O$	Deoxidation reaction rate constant ( $s^{-1}$ )
$M$	Quality of molten steel with decarburization reaction (kg)
$M_C$	Molar mass of carbon (g/mol)
$M_O$	Molar mass of oxygen (g/mol)
$n_{Ar}^b$	Molar amount of argon in the bubble
$n_{CO}^b$	Molar amount of CO generated on the bubble surface (mol)
$N$	Number of gas injection nozzles
$P$	Pressure (Pa)
$P^\ominus$	Standard atmospheric pressure (Pa)
$P_{CO}$	Partial pressure of CO (Pa)
$P_{CO_2}$	Partial pressure of CO <sub>2</sub> (Pa)
$P_{O_2}$	Partial pressure of O <sub>2</sub> (Pa)
$P_{local}$	Local pressure (Pa)
$P_{critical}$	Estimated pressure to overcome for CO bubble nucleation (Pa)
$r_{CO}$	Bubble radius of generated CO (m)
$R$	Constant = 8.314 [J/(mol K)]
$S_{[C]}$	Source term of carbon mass concentration change caused by decarburization reaction
$S_{[O]}$	Source term of oxygen mass concentration change caused by decarbonization reaction and oxygen blowing process
$Sc_t$	Turbulent Schmidt number
$t_e$	Contact time between bubble and molten steel (s)
$T$	Temperature (K)
$u_l$	Velocity of liquid phase (m/s)
$u_b$	Bubble velocity (m/s)
$u_{down}$	Longitudinal velocity of the down-leg snorkel (m/s)
$u_R$	Relative velocity (m/s)
$V_{interior}$	Volume of molten steel with decarburization reaction inside the molten steel ( $m^3$ )
$V_{surface}$	Volume of molten steel with decarburization reaction on the surface of molten steel ( $m^3$ )
$V_{bubble}$	Volume of molten steel at the corresponding position of decarburization reaction of bubbles ( $m^3$ )
$\varepsilon$	Turbulent dissipation rate ( $m^2/s^3$ )

$\mu_t$	Turbulent viscosity [kg/(m s)]
$\rho$	Density (kg/m <sup>3</sup> )
$\sigma_{gl}$	Surface tension between gas and liquid (N/m)

## REFERENCES

1. Y. Shan, J. Miettinen, S. Lei, and S. Louhenkilpi: *Steel Res. Int.*, 2015, vol. 86, pp. 466–77.
2. J. Wei, S. Zhu, and N. Yu: *Ironmaking Steelmaking.*, 2000, vol. 27, pp. 129–37.
3. K. Kleimt: *Metall. Secondaire.*, 1995, vol. 92, pp. 493–502.
4. B. Kleimt, J. Cappel, J. Hoffmann, D. Sheng, and S. Landa: *Revue De Metall.*, 2003, vol. 100, pp. 583–93.
5. H. Ling and L. Zhang: *Metall. Mater. Trans. B.*, 2018, vol. 49B, pp. 2709–21.
6. L. Gao, Z. Shi, Y. Yang, D. Li, G. Zhang, A. Mclean, and K. Chattopadhyay: *Metall. Mater. Trans. B.*, 2018, vol. 49B, pp. 1985–94.
7. T. Kitamura, K. Miyamoto, R. Tsujino, S. Mizoguchi, and K. Kato: *ISIJ Int.*, 1996, vol. 36, pp. 395–401.
8. B. Liu, G. Zhu, H. Li, B. Li, Y. Cui, and A. Cui: *Int. J. Min. Metall. Mater.*, 2010, vol. 17, pp. 22–27.
9. P. Li, Q. Wu, W. Hu, and J. Ye: *J. Iron Steel Res. Int.*, 2015, vol. 22, pp. 63–67.
10. H. Yoshihiko, I. Hiroshi, and S. Yoshiyasu: *Tetsu-to-hagané.*, 1998, vol. 84, pp. 21–26.
11. C. Lin, Y. Liu, C. Chang, J. Feng, C. Tseng, W. Chou, and C. Tai: *China Steel Technical Repot.*, 2016, vol. 29, pp. 8–14.
12. S. Pirker and K. Forstner: *Steel Res. Int.*, 2008, vol. 79, pp. 591–99.
13. D. Zhan, Y. Zhang, Z. Jiang, and H. Zhang: *J. Iron Steel Res. Int.*, 2018, vol. 25, pp. 409–16.
14. T. Kuwabara, K. Umezawa, K. Mori, and H. Watanabe: *Trans. Iron Steel Inst. Jpn.*, 1988, vol. 28, pp. 305–14.
15. S. Inoue, Y. Furuno, T. Usui, and S. Miyahara: *ISIJ Int.*, 1992, vol. 32, pp. 120–25.
16. L. Zhang, X. Jing, J. Li, T. Xu, and K. Cai: *Int. J. Miner. Metall. Mater.*, 1997, vol. 4, pp. 19–23.
17. Y. Park and K. Yi: *ISIJ Int.*, 2003, vol. 43, pp. 1403–09.
18. H. Ling and L. Zhang: *Metall. Mater. Trans. B.*, 2018, vol. 49B, pp. 2963–68.
19. J. Zhang, L. Liu, X. Zhao, S. Lei, and Q. Dong: *ISIJ Int.*, 2014, vol. 54, pp. 1560–69.
20. H. Ling, F. Li, L. Zhang, and A. Conejo: *Metall. Mater. Trans. B.*, 2016, vol. 47B, pp. 1950–61.
21. Y. Luo, C. Liu, Y. Ren and L. Zhang: *Steel Res. Int.*, 2018, pp. 201800048.
22. H. Ling and L. Zhang: *Metall. Mater. Trans. B.*, 2019, vol. 50, pp. 2017–28.
23. C. Liu, H. Duan, and L. Zhang: *Metals.*, 2019, vol. 9, p. 442.
24. J. Zhang: in *Metallurgical Physicochemistry*. Metallurgical Industry Press, 2004, pp. 307–35.
25. H. Suito and R. Inoue: *Trans. Iron Steel Inst. Jpn.*, 1996, vol. 36, pp. 528–36.
26. J. Wang, L. Zhang, T. Wen, Y. Ren, and W. Yang: *Metall. Mater. Trans. B.*, 2021, <https://doi.org/10.1007/s11663-021-02120-x>.
27. Y. Huang, G. Cheng, Q. Wang, S. Li, and W. Dai: *Ironmaking Steelmaking.*, 2019, vol. 47, pp. 655–64.
28. X. Wang: in *Iron and Steel Metallurgy: Steelmaking*. Higher Education Press, 2007.
29. J. Wei, N. Yu, Y. Fan, S. Yang, J. Ma, and D. Zhu: *J of Shanghai University (English Edition).*, 2002, vol. 6, pp. 167–75.
30. D. Geng, J. Zheng, K. Wang, P. Wang, R. Liang, H. Liu, H. Lei, and J.C. He: *Metall. Mater. Trans. B.*, 2015, vol. 46B, pp. 1484–93.

**Publisher's Note** Springer Nature remains neutral with regard to jurisdictional claims in published maps and institutional affiliations.